NeuroImage 269 (2023) 119903

Contents lists available at ScienceDirect

NeuroImage

journal homepage: www.elsevier.com/locate/neuroimage

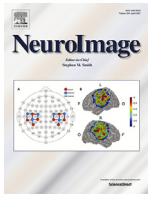

Trigeminal stimulation is required for neural representations of bimodal odor localization: A time-resolved multivariate EEG and fNIRS study

Christine Ida Hucke[a,*], Rebekka Margret Heinen[b], Edmund Wascher[c], Christoph van Thriel[a]

[a] Leibniz Research Centre for Working Environment and Human Factors at the TU Dortmund, Department of Toxicology, Neurotoxicology and Chemosensation, Ardeystrasse 67, 44139 Dortmund, Germany
[b] Ruhr-University Bochum, Institute of Cognitive Neuroscience, Department Neuropsychology, Universitätsstraße 150, 44801 Bochum, Germany
[c] Leibniz Research Centre for Working Environment and Human Factors at the TU Dortmund, Department of Ergonomics, Ardeystrasse 67, 44139 Dortmund, Germany

ARTICLE INFO

Keywords:
EEG
fNIRS
RSA
Spatial representation
Lateralization
Odors
Smell

ABSTRACT

Whereas neural representations of spatial information are commonly studied in vision, olfactory stimuli might also be able to create such representations via the trigeminal system. We explored in two independent multi-method electroencephalography–functional near-infrared spectroscopy (EEG+fNIRS) experiments (n1=18, n2=14) if monorhinal odor stimuli can evoke spatial representations in the brain. We tested whether this representation depends on trigeminal properties of the stimulus, and if the retention in short-term memory follows the "sensorimotor recruitment theory", using multivariate representational similarity analysis (RSA). We demonstrate that the delta frequency band up to 5 Hz across the scull entail spatial information of which nostril has been stimulated. Delta frequencies were localized in a network involving primary and secondary olfactory, motor-sensory and occipital regions. RSA on fNIRS data showed that monorhinal stimulations evoke neuronal representations in motor-sensory regions and that this representation is kept stable beyond the time of perception. These effects were no longer valid when the odor stimulus did not sufficiently stimulate the trigeminal nerve as well. Our results are first evidence that the trigeminal system can create spatial representations of bimodal odors in the brain and that these representations follow similar principles as the other sensory systems.

1. Introduction

Spatial representations – the mental concept of one's environment – have been intensively studied in vision. However, it is reasonable to assume that other senses such as the sense of smell also encompass the ability to create spatial representations (Schifferstein et al., 2009). The difference in nostril concentration can offer spatial information of the odor source in animal models (Baker et al., 2018; Rajan et al., 2006). However, how humans gain spatial information based on smells (Porter et al., 2007; Welge-Lüssen et al., 2014) and how this is reflected in the brain is still under investigation. The most basic form of a spatial information of smells would be an odor presented to one nostril only. We want to investigate how the brain represents this mental spatial information of a lateralized odor stimulus.

While there are odors that are purely olfactory (e.g., phenylethyl alcohol or H_2S) or exclusively trigeminal (CO_2), in humans, the perception of mixed or so-called bimodal odors requires both sensory systems. The respective sensory involvement depends on the concentration of the bimodal odor (Cometto-Muñiz and Abraham, 2016; Hummel, 2000; van Thriel et al., 2006). Lower concentrations of airborne molecules mainly stimulate olfactory receptor neurons. With increasing concentration of the same odor, the trigeminal system becomes stimulated as well. The olfactory system encodes the identity of an odor. The trigeminal system encodes additional odor qualities such as burning, stinging, cooling or pungent sensations (Shusterman, 2009). The trigeminal system triggers repelling reflexes such as sneezing or coughing and thereby protects the organism from inhaling putative harmful substances. Yet another task ascribed to the trigeminal system is transporting spatial information. Is trigeminal activation the basis for spatial representations of bimodal odors in the brain?

A behavioral endpoint demonstrating the potential to create spatial representation of the trigeminal system is the localization task assessing the lateralization threshold. During the assessment, one nostril is stimulated with an increasing concentration of a compound while the other nostril is stimulated with pure air. The threshold at which humans are able to localize the stimulated nostril is the concentration at which the trigeminal system is starting to be involved (Croy et al., 2014; Frasnelli et al., 2009, 2010; Kleemann et al., 2009; Kobal et al., 1989;

* Corresponding author.
E-mail addresses: hucke@ifado.de (C.I. Hucke), rebekka.heinen@ruhr-uni-bochum.de (R.M. Heinen), wascher@ifado.de (E. Wascher), thriel@ifado.de (C. van Thriel).

https://doi.org/10.1016/j.neuroimage.2023.119903.
Received 4 July 2022; Received in revised form 28 November 2022; Accepted 24 January 2023
Available online 25 January 2023.

Smeets et al., 2006). Thus, the involvement of the trigeminal system enables humans to detect spatial information of bimodal odors.

In this study we explore ways of reliably detecting mental or neural representations of simple spatial bimodal odor information in the brain. We contrast left and right nostril stimulations with a bimodal odor in a concentration that is lateralizable while neural signals were recorded with a multi-method electroencephalography (EEG) and functional near-infrared spectroscopy (fNIRS) setup. Attempts have been made to study chemosensory spatial representations by comparing nostril-specific odor stimulations using *univariate* EEG approaches on classical chemosensory event-related potentials (CSERPs). On the level of CSERPs no reliable nostril- or side- effect could be demonstrated across studies (Kobal et al., 1992; Olofsson et al., 2006; Rombaux et al., 2008; Stuck et al., 2006). One drawback of CSERP investigations is the relatively low signal-to-noise ratio.

The use of univariate analyses approaches causes the loss of information that a whole-electrode configuration pattern can provide. This might be the reason why thus far no robust effect of nostril-side nor a representation of spatial information could be demonstrated. To overcome this, more recent *multivariate* analysis strategies on CSERPs show to be more successful in differentiating monorhinal stimulations (e.g., Hucke et al., 2021; Kato et al., 2022; Lascano et al., 2010).

Furthermore, Huart et al., (2012) demonstrated that transforming the signal from the time domain into the time-frequency domain improves the signal robustness and detectability. It was shown that chemosensory stimulations evoke frequency changes in delta (1–4 Hz) and lower theta frequency bands around 5 Hz (Huart et al., 2012; Jiang et al., 2017; Schriever et al., 2017; Yang et al., 2021). In addition to odor identity, these EEG frequencies might encode spatial information i.e., a sensory representation that can differentiate between the nostrils (Invitto et al., 2019).

A putative method to study such representation is "representational similarity analysis" (RSA), a multivariate method to investigate the similarities of neural patterns instead of single electrodes (Haxby et al., 2014; Kriegeskorte et al., 2008; Kriegeskorte and Kievit, 2013). The distinctiveness of a representation can be quantified by contrasting patterns of all electrodes simultaneously of multiple different stimulus types, conditions, or in this case spatial information of an odorant. If the trigeminal nerve enables a stable formation of a spatial representation, there should be distinct neuronal pattern evoked by one-sided/monorhinal stimulations. No such distinction of neural representations should be possible if a non-lateralizable thus below-trigeminal concentration of a compound is being used.

In addition to information from the time-frequency domain it would also be of interest to determine which brain areas are involved in creating spatial representations of odors. fNIRS is an optical imaging technique that assesses the local relative changes of oxygenated (HbO) and deoxygenated (HbR) hemoglobin in selected cortical regions (Jöbsis, 1977). In a previous study we used fNIRS to record hemodynamic responses over the somatosensory areas related to chemical trigeminal stimulation (Hucke et al., 2018). Birhinal stimulation evoked hemodynamic changes around 10 to 15 s post-stimulus in both hemispheres. However, no systematic difference between left- and right-nostril stimulations could be revealed. One reason might have been that the analysis was still channel/region of interest based, thus not exhausting the potential of multivariate approaches investigating a pattern across all channels at the same time.

RSA is a method that can be applied to a variety of methods making this approach a promising contestant for this multimethod recording setup (Kriegeskorte et al., 2008). We wanted to test whether RSA would be applicable to both recording modalities to reveal that spatial representation are formed in the motor-sensory region as recorded using fNIRS and that lower EEG frequencies play a key role in spatial representations. The signal source was estimated to determine the neural generators which play a role in spatial representations of bimodal odors and give rise to the respective frequencies.

To that end, we conducted two independent EEG+fNIRS experiments. In experiment 1 above-lateralization threshold concentrations of acetic acid were monorhinally presented to participants using an olfactometer. We used RSA to test if trials of left- and right-sided stimulations are more similar to each other than to the respective other-sided stimulation. We expected to find these effects in frequencies below 5 Hz in EEG time-frequency data (Huart et al., 2012; Invitto et al., 2019; Schriever et al., 2017). Furthermore, in fNIRS data the total hemoglobin response (HbT=HbO+HbR) was expected to be more similar within a condition opposed to between the conditions starting at around 10 s post stimulus-onset (Hucke et al., 2018; Invitto et al., 2019).

In our previous fNIRS study (Hucke et al., 2018) we postulated that in line with the "sensory recruitment" or "sensorimotor recruitment theory" the representation of which nostril has been stimulated was retained in short-term memory by continuous neuronal activation in the same brain regions as the perception (D'Esposito and Postle, 2015). After each stimulation, the participants were asked to remember the stimulated nostril for a certain period which was accompanied by a stable increased HbO concentration. In the current study we wanted to test if the spatial representation of a bimodal odor stimulus is indeed retained in short-term memory. This should be manifested in a stable representational difference in the fNIRS data until the end of a trial.

Experiment 2 served two purposes: First, it replicated results from experiment 1. Second, it included an additional within-subject condition with lower (above detection but below lateralization) acetic acid concentration next to the high-concentration trials. This served as a proof of concept when applying the RSA to the low-concentration condition with the expectation that no significant RSA results would be achieved.

2. Materials and methods

2.1. Participants

Participants (18 to 35 years) were recruited by means of online advertisements. Exclusion criteria for both experiments entailed migraine, pregnancy, history of neurological or psychiatric diseases, asthma, acute or chronic upper airway diseases, acute allergies, intake of drugs, smoking, and left-handedness or a hairstyle unsuitable for EEG+fNIRS recordings. In case of medication intake, participants were excluded if the compound had potential neurophysiological impact.

At the day of the experiment, participants were required to pass a pulmonary lung function (forced exhaled volume > 80%, MasterScope TP, JAEGER/CareFusion, Höchberg, Germany) and olfactory function test [Sniffin' Sticks identification subtest, Burghart Messtechnik GmbH, Wedel, Germany, (Hummel et al., 2007; Oleszkiewicz et al., 2019)].

2.1.1. Experiment 1

Nineteen participants took part in experiment 1. One participant was excluded since no stimulation with acetic acid was perceived at the start of the experiment and thus the experiment was aborted. The sample description of the 18 participants that entered the analysis is shown in Table 1 in the left column. Half the EEG data of one participant got lost due to recording issues. However, the remaining half of the data was included in the final dataset.

Table 1
Demographic data of the subjects included in the analysis of both experiments.

	Experiment 1	*Experiment 2*
N (female/male)	18 (13/5)	14 (11/3)
Age (years), *M (SD)* *	26.77 (4.74)	22.73 (2.41)
FEV1 %, *M (SD)*	99.04 (10.38)	102.65 (9.83)
Sniffin' Sticks ID, *M (SD)*	13.66 (0.79)	13.00 (1.37)

* Sample differs significantly $p < 0.05$, FEV1: forced expiratory volume in 1 s, ID: identification subtest.

2.1.1. Experiment 2

An independent sample of 15 subjects was invited to participate in experiment 2. One subject aborted the participation on own terms, hence the final sample comprised 14 datasets (right column of Table 1).

2.2. Stimuli and olfactometer

We used the same flow-olfactometer as in the previous studies (Hucke et al., 2018, 2021). Specifically, see (Hucke et al., 2018) for an elaborate description of the device and Hucke et al. (2021) for technical adaptations made in order to optimize the setup for EEG recordings. In short, the olfactometer delivers olfactory stimuli into the participants nostrils and allows for monorhinal stimulations. The device creates a seamless stimulus integration into a constant airflow of 2.5 l/min of clean air. This ensures a precise stimulus on- and offset and purely chemical stimulation of the trigeminal nerve sparring co-activation of mechanoreceptors.

Acetic acid served as the stimulus. For the high concentration a liquid concentration of 30 % v/v was used in both experiments [For airborne concentration measurements see Supplement of (Hucke et al., 2018)]. The low concentration (liquid concentration 3.5% v/v) for experiment 2 was adjusted to be detectable yet not lateralizable as assessed by a pilot testing of experienced lab members (Supplement 2).

As described in Hucke et al. (2021) the olfactometer includes a magnetic stirrer which continuously moves the acetic acid ensuring a constant release of molecules and thereby a stable concentration. Unfortunately, the stirrer produces noise picked up by the EEG system which calls for specific filter settings excluding frequencies above 14 Hz. See 3.2.1 for details.

2.3.1. EEG recording

The EEG signals were recorded from 64 Ag/AgCl active electrodes (ActiCap, Brain Products, Gilching, Germany) which were arranged across the scalp according to the international 10-10 system (Oostenveld and Praamstra, 2001) using the Brain Vision Recorder software (version 1.20) and a BrainAmp DC amplifier (sampling rate 1 kHz, Brain Products, Gilching, Germany). FCz served as an online reference. The signal was online low pass filtered at 250 Hz and saved to a Windows 7 PC. The impedance was kept below 10 kΩ throughout the recording using a high-viscosity electrolyte gel (SuperVisc, EASYCAP GmbH, Herrsching, Germany).

2.3.2. fNIRS recording

The hemodynamic signal changes were recorded and saved to a Windows 10 tablet using a multichannel continuous wave fNIRS system (NIRSport, NIRx Medical Technologies, LLC, Glen Head, NY, USA) with a sampling frequency of 7.81 Hz. The probe configuration of 8 sources ($\lambda_{1|2}$ = 750|850 nm) and 6 detectors took on 10-5 EEG positions in the ActiCap creating a total of 16 symmetrical so-called long channels with a maximal distance of 40 mm (Fig. 1 (A)). Furthermore, each light source was flagged by one short-distance detector, which was integrated into the respective light ring-holder creating eight 8 mm short-separation channels. These channels measure oxygenation changes in superficial tissue that can later be regressed from the overall signal (Yücel et al., 2015). As depicted in Fig. 1(B), the setup was created using the AtlasViewer (Aasted et al., 2015) and tMCimg (Boas et al., 2002) software to maximize the sensitivity to the areas shown to be involved in chemosensory processes in the previous fNIRS study (Hucke et al., 2018). For easier readability we will refer to the areas recorded here as "motor-sensory region" even though the probe setup not only spans the pre- and postcentral gyrus but also part of the superior parietal cortex, the supra-marginal cortex, and parts of the superior temporal lobe.

2.4. Procedure and experimental protocols

The ethics committee of the Leibniz Research Centre for Working Environment and Human Factors at the TU Dortmund approved the experimental protocols. Before the experiments started, participants were fully briefed about the experimental procedure and potentially irritating effects of the stimulation with acetic acid and gave informed written consent. After the lung function and the Sniffin' Sticks test indicated no issues, the nasal flow rate of both nostrils was examined by

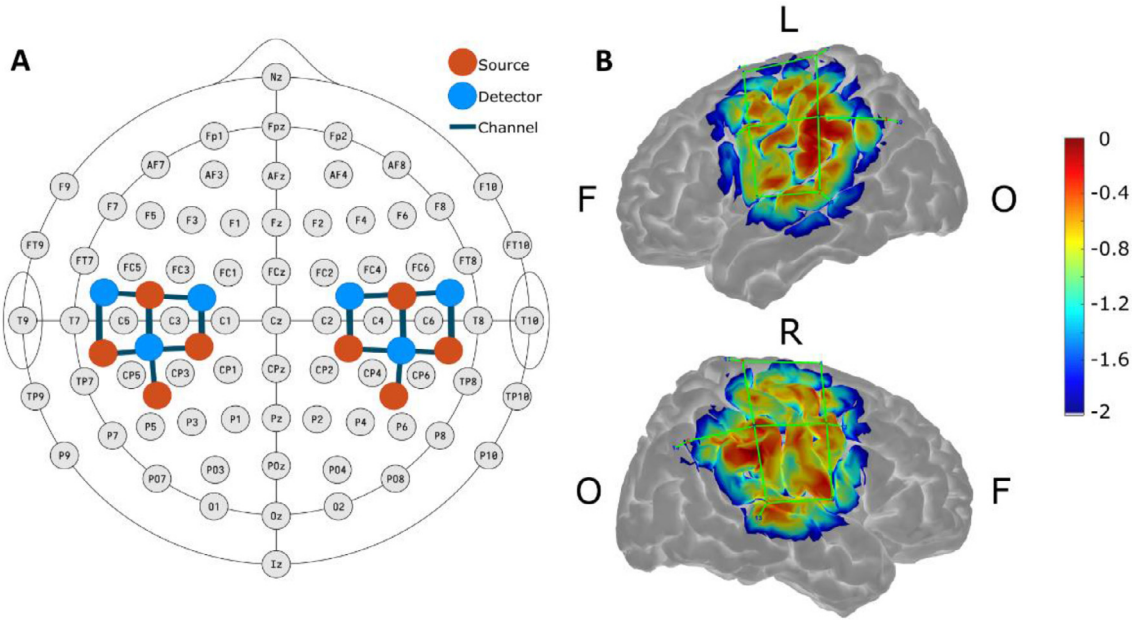

Fig. 1. EEG+fNIRS cap setup. **(A)** EEG electrodes were placed according to the 10-10 setup and fNIRS optodes took on the intermediate 5–10 positions. Red depicts the fNIRS sources and blue the detectors. Each source can pair with multiple detectors to form several channels. In the current setup this results in a total of 16 channels (connecting dark lines). **(B)** Sensitivity profile of the fNIRS channels simulated with AtlasViewer and tMCimg software over the left (L) and right (R) hemispheres. The derived sensitivity values are displayed on a logarithmic scale spanning two orders of magnitude in arbitrary units. Sensitivity at 0 corresponds to high channel sensitivity (red) whereas decreasing values correspond to decreasing sensitivity (blue), respectively. Frontal and occipital lobes are labeled as F and O, respectively. Green lines correspond to the 16 fNIRS channels.

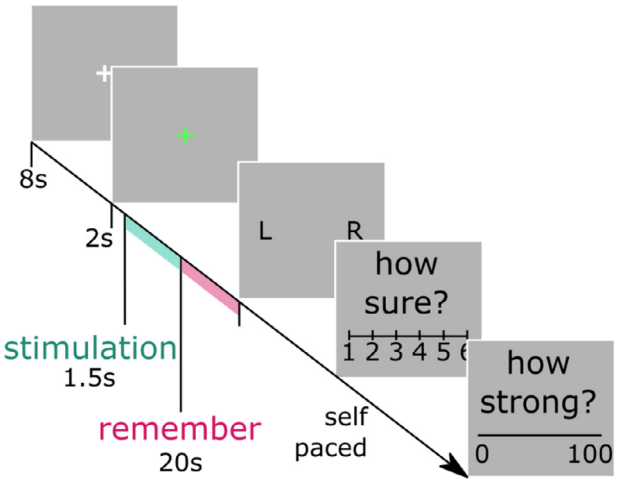

Fig. 2. Trial succession. Each trial started with a baseline and alertness period and was followed by a monorhinal stimulation and a memory phase. Each stimulation was localized, the certainty of localization as well as perceptual strength was rated.

means of an active anterior rhinomanometry (RHINO-SYS, Happersberger otopronst GmbH, Hohenstein, Germany) to determine if participants showed signs of a nasal flow asymmetry. Next, participants were trained in the velopharyngeal closure technique to seal the velum and pharyngeal walls separating the oral and nasal cavities while breathing through the mouth (Kobal, 1981). This ensures a precise stimulus onset as the olfactometer flow is not affected by the participants respiration. After successful training, the EEG+fNIRS cap was put on the participants head, and the signal quality was checked. The cap was further covered with a black opaque showering cap to protect the fNIRS optodes from ambient light. The experiment, which was set up in PsychoPy (Peirce, 2007, 2009) and ran on a Windows 10 Laptop, took place in a dimly lit room where participants were seated in front of a 19" computer monitor and mouse. To keep the alertness levels of the participants as high as possible, the experiment was split into separate parts, which were divided by breaks during which the lights were switched on and the participant could move freely. After the experiment had finished, a second anterior rhinomanometry check-up confirmed the initial nasal flow rate and allowed for the assumption that the nostrils remained unobstructed over the course of the experiment.

2.4.1. Experiment 1 protocol

The experiment comprised 120 trials and was split into two equal parts divided by a break as described above. Thus, each part contained 60 trials, 30 left and right-sided stimulations, respectively. These 60 trials were further divided into blocks of four semi-randomly presented trials (two left and two right). In-between blocks, participants could temporarily switch to nasal breathing and drink water to prevent discomfort due to potential dryness caused by mouth breathing. Participants could individually start the next block via button press. As depicted in Fig. 2, each trial started with a baseline period displaying a white fixation cross in the center of a grey screen. After 8 s, the cross switched to green indicating the imminent stimulus presentation which occurred after 2 s either to the left or to the right nostril. To minimize ocular artifacts in the EEG signal, participants were instructed to refrain from blinking after the fixation cross had turned green for at least until they had confidently perceived a stimulation but for as long as they felt comfortable. Participants were instructed to remember the stimulated side. After ~20 s a series of questions appeared on the screen asking to 1) indicate which side has been stimulated (left, right), 2) evaluate the confidence of the nostril localization on a Likert scale (0-guessed to 7-absolutely certain), and 3) rate the strength of perception on a continuous visual analogue scale ranging from "not perceived at all" to "strongest perception imaginable". All answers were given by means of a mouse click using the right hand. The overall participation time was around 4–5 h for which participants either received 10 €/h or participation credits for their university degree.

2.4.2. Experiment 2 protocol

The total trial amount increased to 240 trials as in addition to the 120 previous trials 120 trials with low concentrations of acetic acid was included (see 2.2) resulting in a within-subject design. From hereon we will refer to "high" and "low" concentrations, respectively. Therefore, experiment 2 was split into four equal parts, each containing 60 trails. Again, the trials were divided into blocks of semi-randomized presentations of the four potential conditions: left and right side, high and low concentration. The trial succession, break policy, and behavioral ratings were kept the same as in experiment 1. Participation time was around 5–6 h, which was reimbursed with 10 €/h or credit points as well.

3. Data processing and analyses

3.1. Data and code availability statement

The datasets generated and/or analyzed during the current study and codes for the analysis are stored in a public OSF repository (https://osf.io/6zmq7/).

3.2. Data preprocessing

3.2.1. EEG preprocessing

The EEG data of experiment 1 was previously analyzed in a different publication (Hucke et al., 2021) where the preprocessing steps are described in more detail. The same preprocessing steps were undertaken for experiment 2 including offline applied Matlab2018b and EEGLAB (v14_1_2b) (Delorme and Makeig, 2004) functions. Before the preprocessing, all triggers were shifted 50 ms to counteract a temporal delay caused by the olfactometer. The concatenated data was band-pass filtered (Hamming windowed sinc FIR band-pass filter, 0.5 Hz to 14 Hz, 0.5 Hz transition band width [Cut-off frequencies: 0.25–14.25 Hz], filter order: 6601). Channels with a normalized kurtosis (20% trimming) exceeding 5 SD of the mean were rejected (average number of rejected channels; experiment 1: 4.61, experiment 2: 5.14 channels per participant). After re-referencing the data to the average signal of the remaining channels the continuous data was epoched from -2000 ms to 6000 ms with respect to the stimulus onset including a baseline correction of 200 ms preceding stimulus onset. An iterative automatic trial rejection procedure (rejection threshold: 1000 μV, detection prob.: 5 SD, max. % of trials rejected/iteration: 5%) was followed by an independent component decomposing the signals into X independent components (ICs) (X = number of remaining channels -1 controlling for the rank deficiency due to the average reference). ICs containing ocular artifacts or generic discontinuities were automatically detected/rejected using the ADJUST (Mognon et al., 2011) and ICLabel (Pion-Tonachini et al., 2019) plugins. Further, a single-equivalent current dipole for each IC was estimated based on the spherical head model (Brain Electrical Source Analysis) as implemented in the DIPTFIT plugin v2.3 (Oostenveld et al., 2003). ICs with a residual variance higher than 40%, locations outside the scalp or that were labeled as < 50% probability of originating from the brain were removed (Average rejection; experiment 1: 14.92, experiment 2: 16.36 ICs). The remaining trails were again checked by the automatic trial rejection procedure with the same parameters (Total average number of rejected trails; experiment 1: 23.83 [19.86%], experiment 2: 48.93 [20.39%]). Lastly, rejected channels were interpolated using the spherical spline interpolation algorithm.

3.2.2. fNIRS preprocessing

fNIRS recordings were processed offline using the Matlab2018b based Homer2 (Huppert et al., 2009) functions. First, long channels with raw data values exceeding $1e^{-7}$ or a signal-to-noise ratio

[*M*(data)/*SD*(data)] lower than 2 were pruned (*enPruneChannels*) and excluded from further analysis. In experiment 1 one subject had 3 missing long channels and another subject had one missing long channel. In experiment 2 three subjects each missed one long channel. Short-separation channels that did not meet the quality criteria as stated above were flagged and needed to be substituted for the regression described below. On average 4.51% of short-separation channels per participant in experiment 1 and 2.90% in experiment 2 were interpolated. Next, the raw intensity signals of all channels were converted to optical density (*hmrIntensity2OD*). Each channel was checked for motion artifacts defined as signal values exceeding 50 SD or 5 μM within 500 ms. Trials were removed if an artifact was within the range of −5 to +10 s around the stimulus onset (*hmrMotionArtifactByChannel, enStimRejection*). In experiment 1 a total of 7 trials and in experiment 2 only 2 trials across participants were excluded. A bandpass filter was applied with a lower cut off at 0.01 and a higher cut off at 0.3 Hz (*hmrBandpassFilt*). The filtered optical density data were converted to HbO, HbR, and the total oxygenation change (HbT) concentration changes using the modified Beer-Lambert Law (Delpy et al., 1988) with a partial path length factor of 6 for both wavelength (*hmrOD2Conc*).

A general linear model (GLM) including the closest short-distance channels as regressors for the long channels was performed in Python 3.7 using the *GLM* function of the statsmodels package. In case the closest short-separation channel was excluded from the analysis due to insufficient data quality, the next most neighboring short-separation channel (or the mean of two if both had the same distance) was used as regressor. The data was z-transformed, and the experimental parts were concatenated.

3.3. Statistical analyses

3.3.1. Behavioral analysis

The behavioral data analysis was conducted in R (RStudio Team (2016), RStudio: Integrated Development for R. RStudio, Inc., Boston; version 1.1.463) using the stats package (R Core Team, version 4.0.3). For all tests significance was determined at an alpha level of 0.05 and, if applicable, non-parametric alternative tests were conducted in case of a significant Shapiro-Wilk test.

In experiment 1, the lateralization ability of the participants was tested using a one-sample *t*-test against a lateralization accuracy at chance level (50%). Furthermore, ratings of lateralization confidence and perceptual strength were each compared against a score of zero using further one-sample *t*-tests. In experiment 2, again one-sample *t*-tests assessed the lateralization accuracies, confidence, and perceptual ratings of the high and low concentration condition, separately. Furthermore, paired *t*-tests compared the respective scores of the two conditions to confirm that the high concentration was indeed lateralized with a higher accuracy and done so with a higher confidence as well as higher perceptual ratings. Lastly, the behavioral data of experiment 1 was compared to the data of the high concentration condition of experiment 2 using independent sample *t*-tests.

3.3.2. Representational Similarity Analysis (RSA)

The RSA on EEG and fNIRS data was conducted in Python (3.7) and R. As depicted in Fig. 4(A), RSA is based on correlation matrixes comparing activity patterns of all electrodes (EEG) or channels (fNIRS) simultaneously across conditions or stimuli. Using this approach, we can study similarities between patterns as well as their distinctiveness. In our study we compared within and between condition patterns. The distinctiveness of neural representations can be quantified by correlating the neural pattern evoked by one-sided trigeminal stimulation and compare this pattern to the pattern of the respective other-sided stimulation. Within condition similarities were computed by correlating all trials of the same condition compared to correlating all trials of one condition with the trials of the respective other condition (between condition correlation) using Spearman's Rho.

Data of experiment 1 were used to test the initial hypotheses of relevant time-frequency points in EEG data and time windows in fNIRS data. The aim was to determine time (and time-frequency) windows in which the neural patterns of left trials are more similar to the pattern of all other left trials compared to the pattern of right trials and vice versa. To evaluate the transferability to another dataset the same approach was applied to the high-concentration trials of experiment 2. As a proof of concept that the results were indeed related to trigeminal stimulation as opposed to olfactory processes, the RSA was applied to the low-concentration trials in a following step.

3.3.3. EEG RSA

To analyze time-frequency data using RSA, the neural activation pattern (all channels) in each frequency in each time window of one condition/stimulus is compared to the pattern of the others (e.g., Fellner et al., 2020; Liu et al., 2020). More precisely, for each participant, the preprocessed EEG data of all channels was sectioned into 28 frequency bins and 24 time bins. To that end, a Hamming windowed bandpass fir-filter with zero padding [4 cycles; (Gramfort et al., 2013)] iteratively passed the 28 linearly spaced frequency bands from 0.3 to 14 Hz. In each iteration, thus for each frequency band, epochs ranging from –500 to 3000 ms around a stimulus onset were extracted. Each frequency-filtered epoch was sectioned into 24 equally spaced time bins. We then correlated the neural activation pattern of each time bin (145 ms × 64 channel) to the neural activation patterns of that time bin of all other left and all other right trials, thereby generating *one* data point representing the within condition similarity and *one* representing the between condition similarity. Correlations were Fisher Z-transformed and the difference of within and between correlations was computed. Across participants, in each bin a one-sided one-sample *t*-test against a correlation difference of 0 rendered an overall 24 × 28 time-frequency *t*-map. *T*-clusters of neighboring (and diagonal) bins with a *p*-value below 0.05 were extracted. The *t*-values of each cluster were summed up creating a so-called cluster mass. The cluster mass of each cluster was compared against a surrogate distribution of 10,000 permutations to determine whether it exceeded values that were expected under the null hypothesis. To create the surrogate distribution, the time bins were shuffled (keeping the frequencies stable) in each permutation and a *t*-statistic was performed as described for the real data. Again, cluster masses of continuous clusters were created. Only the largest cluster mass was kept of each permutation. The surrogate cluster masses were ranked including the empirical cluster mass of the real data. The number of surrogate values larger than the real empirical cluster mass was divided by the 10,000 permutations to create the respective *p*-value.

3.3.4. EEG source localization

The overarching common sources were localized on a merged dataset including experiment 1 and high-concentration trials from experiment 2. The source estimation was performed using Dynamic Imaging of Coherent Sources (DICS; van Vliet et al., 2018) beamformer spatial filters [implemented in MNE, v1.2.2, (Gramfort et al., 2013)]. In each subject, the raw data was epoched and the cross-spectral density (CSD) was computed using morlet wavelets (4 cycles). The forward solution was based on the 10-10 EEG positions and brain template (fsaverage, FreeSurfer; Fischl, 2012). The spatial filters were applied to the CSD matrix during the time range determined by the RSA (400 ms to 2400 ms). The resulting source power was normalized to the estimated baseline source power. The group average was thresholded exporting the top 10% source power values. The thresholded group averages were labeled according to the Automated Anatomical Labelling atlas (Tzourio-Mazoyer et al., 2002).

3.3.5. fNIRS RSA

Preprocessed fNIRS data of all channels was epoched (trial onset to 20 s) and baseline corrected (- 5 s). Similar to the EEG RSA, for each time

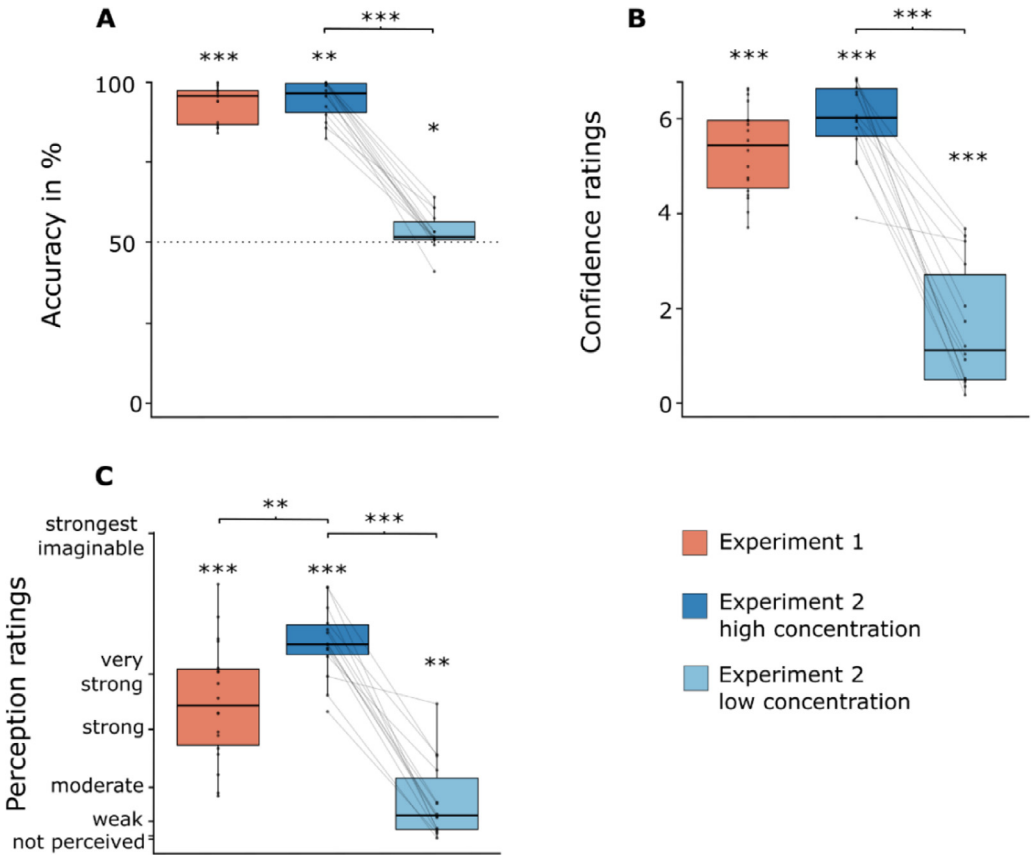

Fig. 3. Boxplos showing behavioral results across both experiments, split according to concentration in experiment 2. **(A)** Lateralization accuracies of monorhinal stimulations. The dotted line represents chance level of 50%. **(B)** Confidence ratings of participants judging the certainty of lateralization response. Ratings range from 0 ("guessed") to 7 ("absolutely certain"). **(C)** Perception ratings displayed on a logarithmically anchored labeled magnitude scale (Green et al., 1996) ranging from "not perceived at all" to "strongest perception imaginable". Dots show descriptive means for each subject; individual observations are linked with lines. * $p < 0.05$, ** $p < 0.01$, *** $p < 0.001$.

point the fNIRS trials within and between each condition were correlated using Spearman's Rho. Resulting correlation matrices were Fisher Z-transformed. The means of within and between correlations were statistically compared using a 10,000-fold Monte Carlo permutation test in R [*symmetry_test*, coin package, (Zeileis et al., 2008)].

3.4. Supplementary analysis

The same analysis was performed on combined data of experiment 1 and high concentration condition trials from experiment 2 to explore the generalizability and stability of the effects (Supplement 1).

4. Results

4.1. Behavioral results

Behavioral results of experiment 1 have been published in a previous publication (Hucke et al., 2021). In experiment 1, where only high concentration of acetic acid was administered to the participants, lateralization accuracies ($M = 93.47\%$, $SD = 5.71$, $Median = 95.83\%$, $IQR = 86.88$–97.50%) significantly exceeded chance levels of 50 %, $Z = 3.71$, $p < 0.001$, effect size r[1] $= 0.87$ (Fig. 3 (A)). Participants were confident in their lateralization abilities as evident by a significantly higher (range: 0–7, $M = 5.35$, $SD = 0.94$) than zero rating, $t(17) = 24.13$, $p < 0.001$ (Fig. 3(B)). With regard to the perceived strength of stimulation, participants evaluated their perception (transformed range 0–100: $M = 44.98$, $SD = 19.58$) as being significantly stronger than "not perceived at all", $t(17) = 9.75$, $p < 0.001$ (Fig. 3(C)). The average score was equivalent to an LMS-scale anchor between "strong" and "very strong" (Green et al., 1996).

In experiment 2 participants were exposed to high (same concentration as experiment 1) and low concentrations of acetic acid. Lateralization scores of high concentration trials ($M = 94.70\%$, $SD = 6.01$, $Median = 96.67$, $IQR = 90.62$–99.79%) significantly exceeded chance levels, $Z = 3.27$, $p = 0.001$, effect size $r = 0.88$. Opposed to our assumption participants were also able to lateralize the low concentration trials, $t(13) = 2.16$ (two-sided), $p = 0.05$, yet with a significantly lower accuracy ($M = 53.39$ %, $SD = 5.87$) than the high concentration trials, $t(13) = 18.84$, $p < 0.001$ (Fig. 3(A)). Participants were confident in their ratings in high ($M = 5.99$, $SD = 0.85$) and low ($M = 1.61$, $SD = 1.29$, $Median = 1.13$, $IQR = 0.50$-2.72) trials both exceeding ratings of zero, $t_{high}(13) = 26.37$, $p_{high} < 0.001$, $Z = 3.26$, $p_{low} < 0.001$, effect size $r = 0.87$. However, participants were significantly more confident in lateralizing high concentration trials compared to low concentration trials, $t(13) = 9.93$ $p < 0.001$ (Fig. 3(B)). Perceptual ratings for high ($M = 64.30$, $SD = 11.71$) and low ($M = 13.13$, $Median = 8.10$, $SD = 12.81$, $IQR = 3.54$-20.19) trials suggested that both stimulations were indeed perceived as indicated by a significantly greater that zero rating, $t_{high}(13) = 20.54$, $p_{high} < 0.001$; $Z_{low} = 3.26$, $p_{low} = 0.001$, effect size $r = 0.87$. High concentration trials were rated as significantly stronger (between "very strong" and "strongest imaginable") as op-

[1] The effect size r is calculated as Z statistic divided by the square root of the sample size (N) (Z/sqrt(N)).

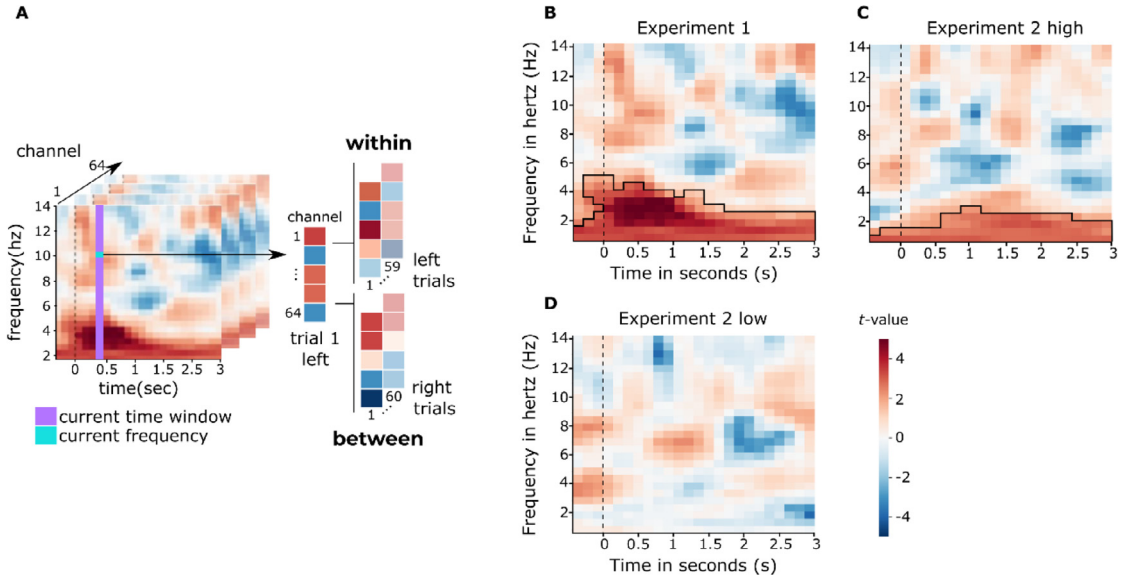

Fig. 4. **(A)** Description of RSA on EEG time-frequency data. The pattern across all EEG channels at each time point within a frequency band is correlated with the same-sided trials (within correlation) and respective other-sided trials (between correlation). *t*-maps of testing the within-between correlation difference against zero for **(B)** experiment 1, experiment 2 **(C)** high and **(D)** low concentrations separately. Positive *t*-values indicate a higher within-condition compared to between-condition similarity (Scales -5 - 5). The dotted line indicates the stimulation onset. The black lines encapsulate clusters that pass the significance threshold and were compared against the 10,000-fold surrogate distribution in the consecutive analysis step.

posed to low concentration trials (between "weak" and "moderate"), $t(13) = 11.48$, $p < 0.001$ (Fig. 3(C)).

Comparing the behavioral data from experiment 1 to high condition trials of experiment 2 showed that the lateralization accuracies did not differ, $Z = -0.78$, $p = 0.43$, effect size $r = 0.14$ (Fig. 3(A)). Also confidence ratings did not differ significantly, $t(29.25) = -2.03$, $p = 0.052$ (Fig. 3(B)). Interestingly, perceptual ratings differed significantly across the two experiments, even though the same concentration was used, $t(28.39) = -3.47$, $p = 0.002$. Participants evaluated the stimulations as stronger in experiment 2 compared to experiment 1 as can be seen in Fig. 3(C).

4.2. RSA EEG results

One-sided *t*-tests against zero comparing the difference of within and between condition correlations rendered a time-frequency *t*-map (Fig. 4). Stronger within-condition correlations in expected low frequency ranges up to 5 Hz can already be suspected in experiment 1 (Fig. 4(B)) and in high but not in low concentration trials of experiment 2 (Fig. 4(C) and (D)). In the following step, clusters surpassing the 0.05 threshold (see 3.2.3) were extracted and compared against the 10,000-fold surrogate distribution to determine if they are statistically significant.

The temporal information of the continuous frequency band below 1 Hz from trial onset to trial offset should be interpreted with care. Due to the very low frequencies, the temporal precision is diminished after the time-frequency convolution. However, temporal information can be gathered in frequencies from 1 to about 5 Hz. For experiment 1 the permutation test showed that the *t*-cluster in the low frequency range persisted ($p < 0.001$) (Fig. 5 (A)). In the time range from stimulus onset to around 1400 ms a clear peak can be detected at around 500 ms with the peak frequency of 2 Hz. This is in line with our expected time (Schriever et al., 2017) and frequency (Huart et al., 2012) range.

In experiment 2 in the high trials a similar, yet slightly time-shifted pattern appeared (Fig. 5(B)). Next to the time-smeared very low frequency band, the permutation *t*-test revealed a cluster in low frequency range up to 3 Hz. This cluster starts around 600 ms with its maximum peak at around 2 Hz between 1600 and 1800 ms post-stimulus onset. This means that within this time range the neural pattern evoked by same-sided stimulation were more similar to each other than to the respective other nostril-stimulations. As expected, in the low concentration condition, no cluster remained as indicated by a non-significant permutation test ($p = 0.14$). This result shows that there was no difference in neuronal patterns correlations within and between each condition.

4.3. Source localization results

The RSA on time-frequency EEG data rendered a significant cluster starting at around 400 ms ranging until at least 2.4 s post stimulus which offered the basis to estimate the delta frequency source (0.5 to 4 Hz). The common estimated sources are displayed in Fig. 5(C). The labeled areas could be grouped to a large cluster in the anterior and posterior cingulate gyrus. Another group of areas correspond to classical olfactory regions (olfactory cortex, amygdala, parahippocampal gyrus). A third region cluster spanned the sensory-motor areas (e.g. pre- and postcentral gyri) and a further broader source was estimated in the frontal region centering around the orbitofrontal gyrus. A final cluster was localized in the occipital cortex (calcerine, lingual, and fusiform gyrus).

4.4. RSA fNIRS results

The HbT values recorded over the somatosensory region evoked by trials of the same condition and between conditions were correlated at each sampling point. A Monte-Carlo permutation test comparing the within and between condition correlation revealed a significantly higher within-condition correlation in experiment 1 at around 13 s post stimulus onset, $p < 0.05$ (Fig. 6 (A)). This significant difference persisted until trial-offset. A similar progression of within and between condition correlation was found in experiment 2 for the high concentration condition (Fig. 6(B)). However, the significant difference started earlier at 10 s post-stimulus onset yet also remained stable until the end of the trials, $p < 0.05$. As expected, no significant difference could be revealed in the low concentration condition, $p > 0.15$ (Fig. 6(C)).

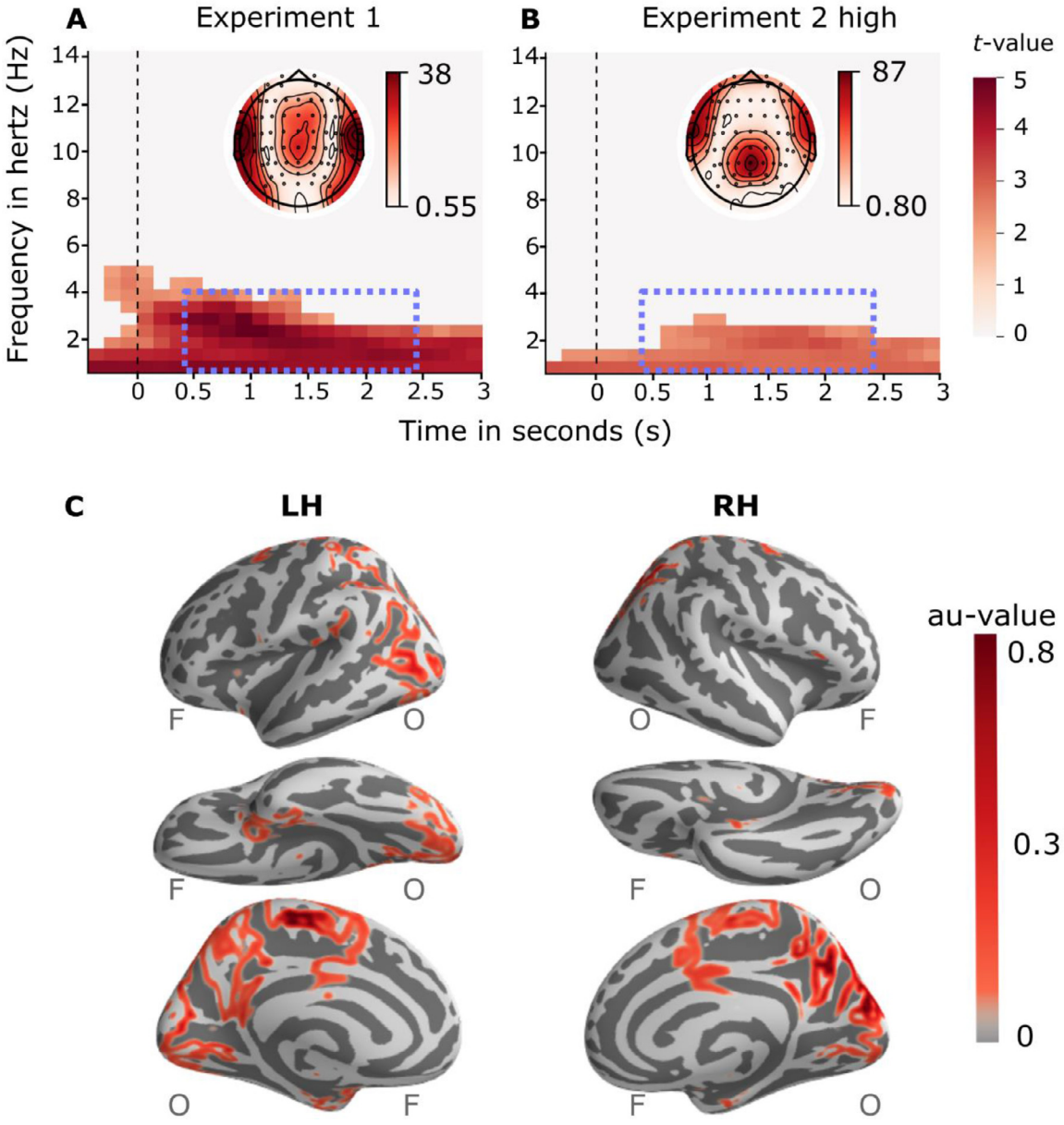

Fig. 5. Permutation results comparing the experimental data clusters against a 10,000-fold surrogate distribution of **(A)** experiment 1 and **(B)** high concentration trials of experiment 2. The dotted line indicates the stimulation onset. Embedded in each cluster plot is the topographical distribution of delta frequencies in the indicated blue rectangles. **(C)** Common delta source activation units (au) as localized using beamformer spatial filter based on the merged data of experiment 1 and high concentration trials of experiment 2.

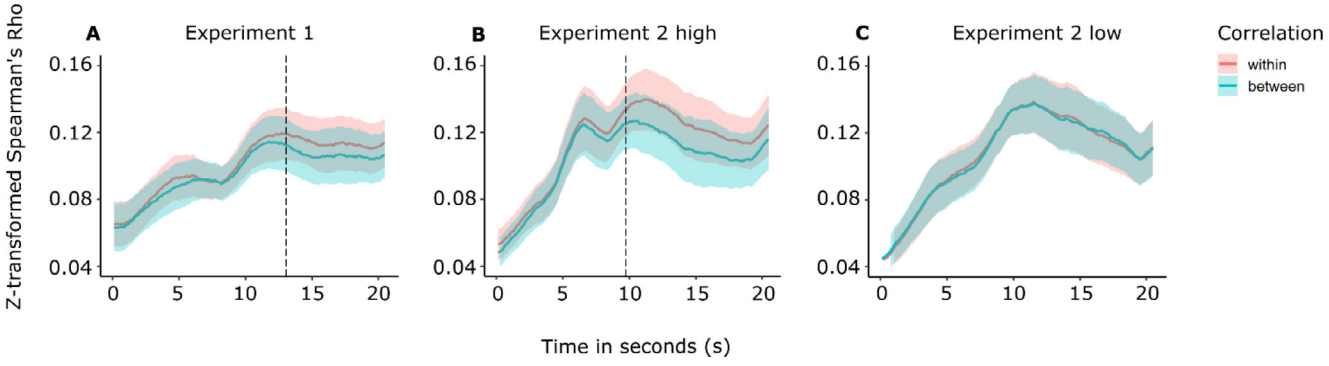

Fig. 6. Results of Monte-Carlo permutation test comparing the within (red) and between (cyan) condition correlation over time of **(A)** experiment 1, **(B)** experiment 2 high and **(C)** low concentration trials. Shaded areas correspond to standard error around the mean. The dotted line indicates the onset of significant within-between condition correlation differences.

5. Discussion

In this study we demonstrated that humans can gain spatial information from bimodal odors and that the emerging mental representation is reflected in activation patterns in the brain. We could show that high concentration stimulations evoke neural patterns that are distinct with regard to nostril-side as measured using fNIRS signals from motor-sensory regions. Moreover, we demonstrated that delta EEG frequency localized in a network including olfactory and motor-sensory regions carry basic spatial information as well. Concentrations of the odorant below the trigeminal threshold did no longer yield distinct neural representations in neither method. This is evidence that trigeminal stimulation is required for a spatial representation of bimodal odor perception as assessed with EEG and fNIRS using RSA.

Our results add more context to previous studies showing trigeminally evoked signals in EEG frequencies up to around 5 Hz (Huart et al., 2012; Schriever et al., 2017). We could demonstrate that these frequencies across the scull entail spatial information of which nostril has been stimulated, thus connecting the rhythmic brain activity to an actual behavioral endpoint.

Arabkheradmand et al. (2020) demonstrated in an intracranial EEG (iEEG) study that the phase of delta oscillations reset in the piriform cortex in anticipation of an olfactory stimulus. The piriform cortex - part of the olfactory network and a source of the delta band in our study - is a key brain area for olfaction (Lundström et al., 2011). The delta phase reset predicted a higher detection accuracy as well as stronger odor evoked theta power. It is possible that this phase reset might entail an emerging spatial representation supporting odor detection which was then represented by the theta power. Jiang et al. (2017) also demonstrated in an iEEG study that low theta oscillations (4–5 Hz) are evoked by olfactory perception in the piriform cortex. Based on this low theta frequency they could decode, which out of four odors was presented. Thereupon, Yang et al. (2021) showed in a consecutive iEEG study that the interplay of theta and gamma oscillations encode the sequence of distinct odors, thus encoding the “what” and “when” of odor perceptions. Our data suggest that delta frequencies might add the ”where” and that this information is dependent on the trigeminal properties of a bimodal odor.

This idea is supported by an auditory study by Bednar and Lalor (2018) who decoded spatial auditory sound location and trajectory based on EEG patterns, specifically from the phase of the delta frequency band. The spatial representation of sensory cues across modalities are perhaps similarly processed using overarching neural oscillations in slow frequency bands. This is supported by an EEG+fNIRS study by Invitto et al. (2019) demonstrating that the delta EEG frequency plays a crucial role in olfactory processing, olfactory-haptic multimodal integration, and neural representation of external world objects. This object representation including odor qualities might also entail spatial trigeminal information as suggested by the results of our study. Our source localization of delta power rendered a broader network including olfactory regions but also other sensory regions such as the occipital lobe and motor-sensory regions. This network might assist spatial sensory integration across modalities based on delta frequencies.

The recruitment of motor-sensory regions in fNIRS demonstrates their involvement in the formation of spatial representations of bimodal odors. The time point at which the neural representations in the fNIRS data become distinct is in line with our previous study (Hucke et al., 2018) showing trigeminally evoked effects at around 10 s post-stimulus onset. fNIRS results from the above-mentioned EEG+fNIRS study by Invitto et al. (2019) demonstrate a correlation between EEG delta power and fNIRS activity in somatosensory regions. This correlation of EEG and fNIRS suggests that effects found in our study, based on separate RSA for EEG and fNIRS, might capture related processes.

The involvement of motor-sensory regions in forming a mental representation is in line with the idea of by Frasnelli et al. (2012). Their framework suggests a functional division for smell processing into ventral and dorsal neural streams. This division has previously mostly been argued for vision. The dorsal stream is thought to process “where” a target is as opposed to identifying an object, ascribed to the ventral or “what” pathway. Frasnelli et al. (2012) demonstrated that these pathways might also apply to bimodal odor perception and localization. Since the areas covered by our fNIRS setup are part of the dorsal stream, the current results support the idea that these areas to are involved in the formation of a spatial “where” representation of bimodal odors.

Furthermore, our results are in line with the “sensorimotor recruitment theory” (D’Esposito and Postle, 2015) implying that the same brain regions which initially process sensory information i.e., motor-sensory regions, retain a representation by continuously firing for the duration of a retention time (Hucke et al., 2018; Lötsch et al., 2012). The similarity within one-sided stimulation compared to the respective other sided stimulation remained significantly distinct until the end of a trial. This finding opens the field to memory representation research as odor stimuli are oftentimes used to cue memories e.g., in targeted memory recall settings. Yet, the memory processes such as rehearsal of odor cues in short-term memory have gained more attention only recently (Yang et al., 2021).

Unfortunately, we could only investigate memory effects in fNIRS and not our EEG data. The study by Yang et al. (2021) demonstrates the crucial role of gamma frequencies in olfactory short-term memory which needed to be filtered out of the data in this study to correct for electromagnetic noise of the olfactometer. Future studies should include a broader range of frequencies with a focus on high frequency bands such as gamma. Moreover, our sample consisted of mostly female participants which might have introduced unknown biases, since previous studies have shown differences in sex with females outperforming men in olfactory measures such as identification, detection, and discrimination (Sorokowski et al., 2019). Lundström et al. (2005) further demonstrated that women were more sensitive to trigeminal stimuli and showed shorter CSERPs latencies than men. Future studies could specifically target sex differences in multivariate EEG or fNIRS studies by collecting larger, balanced samples.

Overall, we could demonstrate that RSA is a good measure for EEG+fNIRS data to explore trigeminally mediated spatial information yielding consistent effects across experiments and data types. In future studies, it would be interesting to administer a more gradient odor concentration, which was not possible with the current study setup. More elaborate olfactometers which can alter the concentration continuously might be used to test the performance of RSA when passing the individual lateralization threshold. Furthermore, the addition of other substances that are purely trigeminal (CO_2) or purely olfactory (e.g., phenylethyl alcohol) might offer further support for our interpretation of RSA results in the low concentration condition. Further, it is possible to modulate this study setup making it wireless, since the fNIRS system used here can be made completely mobile and combined with a mobile EEG. Thus, this study can be seen as the basic foundation for future studies investigating more complex odor-related spatial tasks or even navigational questions in a mobile open field environment.

Human ethics statements

The ethics committee of the Leibniz Research Centre for Working Environment and Human Factors at the TU Dortmund approved the experimental protocols. Before the experiments started, participants were fully briefed about the experimental procedure and potentially irritating effects of the stimulation with acetic acid and gave informed written consent.

Funding

This research did not receive any specific grant from funding agencies in the public, commercial, or not-for-profit sectors.

Declaration of Competing Interests

The authors declare no competing interests.

Credit authorship contribution statement

Christine Ida Hucke: Conceptualization, Methodology, Validation, Formal analysis, Investigation, Data curation, Writing – original draft, Writing – review & editing, Visualization, Project administration. **Rebekka Margret Heinen:** Validation, Formal analysis, Data curation, Writing – review & editing, Visualization. **Edmund Wascher:** Resources, Writing – review & editing. **Christoph van Thriel:** Conceptualization, Methodology, Resources, Writing – review & editing, Supervision, Project administration.

Data Availability

Data and code are available in the author's OSF repository (https://osf.io/6zmq7/).

Acknowledgments

We thank M. Porta and J. Reinders for the preparation of the acetic acid and N. Koschmieder for her assistance during the data acquisition.

Supplementary materials

Supplementary material associated with this article can be found, in the online version, at doi:10.1016/j.neuroimage.2023.119903.

References

Aasted, C.M., Yücel, M.a., Cooper, R.J., Dubb, J., Tsuzuki, D., Becerra, L., Petkov, M.P., Borsook, D., Dan, I., Boas, D.A., 2015. Anatomical guidance for functional near-infrared spectroscopy: atlasviewer tutorial. Neurophotonics 2 (2), 020801. doi:10.1117/1.NPh.2.2.020801.

Arabkheradmand, G., Zhou, G., Noto, T., Yang, Q., Schuele, S.U., Parvizi, J., Gottfried, J.A., Wu, S., Rosenow, J.M., Koubeissi, M.Z., Lane, G., Zelano, C., 2020. Anticipation-induced delta phase reset improves human olfactory perception. PLoS Biol. 18 (5), 1–26. doi:10.1371/journal.pbio.3000724.

Baker, K.L., Dickinson, M., Findley, T.M., Gire, D.H., Louis, M., Suver, M.P., Verhagen, J.V., Nagel, K.I., Smear, M.C., 2018. Algorithms for olfactory search across species. J. Neurosci. 38 (44), 9383–9389. doi:10.1523/JNEUROSCI.1668-18.2018.

Bednar, A., Lalor, E.C., 2018. Neural tracking of auditory motion is reflected by delta phase and alpha power of EEG. NeuroImage 181, 683–691. doi:10.1016/j.neuroimage.2018.07.054.

Boas, D.A., Culver, J.P., Stott, J.J., Dunn, A.K., 2002. Three dimensional Monte Carlo code for photon migration through complex heterogeneous media including the adult human head. Opt. Express 10 (3), 159–170.

Cometto-Muñiz, J.E., Abraham, M.H., 2016. Dose–response functions for the olfactory, nasal trigeminal, and ocular trigeminal detectability of airborne chemicals by humans. Chem. Sens. 41 (1), 3–14. doi:10.1093/chemse/bjv060.

Croy, I., Schulz, M., Blumrich, A., Hummel, C., Gerber, J., Hummel, T., 2014. Human olfactory lateralization requires trigeminal activation. NeuroImage 98, 289–295. doi:10.1016/j.neuroimage.2014.05.004.

Delorme, A., Makeig, S., 2004. EEGLAB: An open source toolbox for analysis of single-trial EEG dynamics including independent component analysis. J. Neurosci. Methods 134 (1), 9–21. doi:10.1016/j.jneumeth.2003.10.009.

Delpy, D.T., Cope, M., van der Zee, P., Arridge, S., Wray, S., Wyatt, J., 1988. Estimation of optical pathlength through tissue from direct time of flight measurement. Phys. Med. Biol. 33 (12), 1433–1442. doi:10.1088/0031-9155/33/12/008.

D'Esposito, M., Postle, B.R, 2015. The cognitive neuroscience of working memory. Annu. Rev. Psychol. 66, 115–142. doi:10.1146/annurev-psych-010814-015031.

Fellner, M.C., Waldhauser, G.T., Axmacher, N., 2020. Tracking selective rehearsal and active inhibition of memory traces in directed forgetting. Curr. Biol. 30 (13), 2638–2644. doi:10.1016/j.cub.2020.04.091, e4.

Fischl, B., 2012. FreeSurfer. NeuroImage 62 (2), 774–781. doi:10.1016/j.neuroimage.2012.01.021.

Frasnelli, J., Charbonneau, G., Collignon, O., Lepore, F., 2009. Odor localization and sniffing. Chem. Sens. 34 (2), 139–144. doi:10.1093/chemse/bjn068.

Frasnelli, J., La, V., Ariza, B., Collignon, O., Lepore, F., 2010. Localisation of unilateral nasal stimuli across sensory systems. Neurosci. Lett. 478, 102–106. doi:10.1016/j.neulet.2010.04.074.

Frasnelli, J., Lundström, J.N., Schöpf, V., Negoias, S., Hummel, T., Lepore, F., 2012. Dual processing streams in chemosensory perception. Front. Hum. Neurosci. 6 (October), 1–9. doi:10.3389/fnhum.2012.00288.

Gramfort, A., Luessi, M., Larson, E., Engemann, D., Strohmeier, D., Brodbeck, C., Goj, R., Jas, M., Brooks, T., Parkkonen, L., Hämäläinen, M., 2013. MEG and EEG data analysis with MNE-Python. Front. Neurosci. 7. https://www.frontiersin.org/articles/10.3389/fnins.2013.00267.

Green, B.G., Dalton, P., Cowart, B., Shaffer, G., Rankin, K., Higgins, J., 1996. Evaluating the "labeled magnitude scale" for measuring sensations of taste and smell. Chem. Sens. 21 (3), 323–334.

Haxby, J.V., Connolly, A.C., Guntupalli, J.S., 2014. Decoding neural representational spaces using multivariate pattern analysis. Annu. Rev. Neurosci. 37, 435–456. doi:10.1146/annurev-neuro-062012-170325.

Huart, C., Legrain, V., Hummel, T., Rombaux, P., Mouraux, A., 2012. Time-frequency analysis of chemosensory event- related potentials to characterize the cortical representation of odors in humans. PLoS ONE 7 (3). doi:10.1371/journal.pone.0033221.

Hucke, C.I., Heinen, R.M., Pacharra, M., Wascher, E., van Thriel, C., 2021. Spatiotemporal processing of bimodal odor lateralization in the brain using electroencephalography microstates and source localization. Front. Neurosci. 14, 620723. doi:10.3389/fnins.2020.620723.

Hucke, C.I., Pacharra, M., Reinders, J., van Thriel, C., 2018. Somatosensory response to trigeminal stimulation: a functional near-infrared spectroscopy (fNIRS) study. Sci. Rep. 8 (1), 13771. doi:10.1038/s41598-018-32147-1.

Hummel, T., 2000. Assessment of intranasal trigeminal function. Int. J. Psychophysiol. 36 (2), 147–155. doi:10.4193/Rhin15.002.

Hummel, T., Kobal, G., Gudziol, H., Mackay-Sim, A., 2007. Normative data for the "Sniffin' Sticks" including tests of odor identification, odor discrimination, and olfactory thresholds: an upgrade based on a group of more than 3000 subjects. Rhinology 264, 237–243. doi:10.1007/s00405-006-0173-0.

Huppert, T.J., Diamond, S.G., Franceschini, M.A., Boas, D.A., 2009. HomER: a review of time-series analysis methods for near-infrared spectroscopy of the brain. Appl. Opt. 48 (10), D280–D298. doi:10.1016/j.drugalcdep.2008.02.002.A.

Invitto, S., Montinaro, R., Ciccarese, V., Venturella, I., Fronda, G., Balconi, M., 2019. Smell and 3D haptic representation: a common pathway to understand brain dynamics in a cross-modal task. A pilot OERP and fNIRS study. Front. Behav. Neurosci. 13 (September), 1–9. doi:10.3389/fnbeh.2019.00226.

Jiang, H., Schuele, S., Rosenow, J., Zelano, C., Parvizi, J., Tao, J.X., Wu, S., Gottfried, J.A., 2017. Theta oscillations rapidly convey odor-specific content in human piriform cortex. Neuron 94 (1), 207–219. doi:10.1016/j.neuron.2017.03.021, e4.

Jöbsis, F., 1977. Noninvasive, infrared monitoring of cerebral and myocardial oxygen sufficiency and circulatory parameters. Science 198 (4323), 1264–1267.

Kato, M., Okumura, T., Tsubo, Y., Honda, J., Sugiyama, M., Touhara, K., Okamoto, M., & Gazzaniga, M. S. (2022). *Spatiotemporal dynamics of odor representations in the human brain revealed by EEG decoding.* https://doi.org/10.1073/pnas

Kleemann, A.M., Albrecht, J., Schöpf, V., Haegler, K., Kopietz, R., Hempel, J.M., Linn, J., Flanagin, V.L., Fesl, G., Wiesmann, M., 2009. Trigeminal perception is necessary to localize odors. Physiol. Behav. 97 (3–4), 401–405. doi:10.1016/j.physbeh.2009.03.013.

Kobal, G., 1981. Elektrophysiologische Untersuchungen des menschlichen Geruchssinns. Thieme Verlag.

Kobal, G., Hummel, T., Van Toller, S., 1992. Differences in human chemosensory evoked potentials to olfactory and somatosensory chemical stimuli presented to left and right nostrils. Chem. Sens. 17 (3), 233–244.

Kobal, G., Van Toller, S., Hummel, T., 1989. Is there directional smelling? Experientia 45, 130–132.

Kriegeskorte, N., Kievit, R.A., 2013. Representational geometry: integrating cognition, computation, and the brain. Trends Cognit. Sci. 17 (8), 401–412. doi:10.1016/j.tics.2013.06.007.

Kriegeskorte, N., Mur, M., Bandettini, P., 2008. Representational similarity analysis - connecting the branches of systems neuroscience. Front. Syst. Neurosci. 2 (4), 1–28. doi:10.3389/neuro.06.004.2008.

Lascano, A.M., Hummel, T., Lacroix, J.S., Landis, B.N., Michel, C.M., 2010. Spatio-temporal dynamics of olfactory processing in the human brain: an event-related source imaging study. Neuroscience 167 (3), 700–708. doi:10.1016/j.neuroscience.2010.02.013.

Liu, J., Zhang, H., Yu, T., Ni, D., Ren, L., Yang, Q., Lu, B., Wang, D., Heinen, R., Axmacher, N., Xue, G., 2020. Stable maintenance of multiple representational formats in human visual short-term memory. Proc. Natl. Acad. Sci. 117 (51), 32329–32339. doi:10.1073/pnas.2006752117.

Lötsch, J., Walter, C., Felden, L., Preibisch, C., Nöth, U., Martin, T., Anti, S., Deichmann, R., Oertel, B.G., 2012. Extended cortical activations during evaluating successive pain stimuli. Soc. Cognit. Affect. Neurosci. 7 (6), 698–707. doi:10.1093/scan/nsr042.

Lundström, J.N., Boesveldt, S., Albrecht, J., 2011. Central processing of the chemical senses: an overview. ACS Chem. Neurosci. 2 (1), 5–16. doi:10.1021/cn1000843.

Lundström, J.N., Frasnelli, J., Larsson, M., Hummel, T., 2005. Sex differentiated responses to intranasal trigeminal stimuli. Int. J. Psychophysiol. 57 (3), 181–186. doi:10.1016/j.ijpsycho.2005.01.003.

Mognon, A., Jovicich, J., Bruzzone, L., Buiatti, M., 2011. ADJUST: an automatic EEG artifact detector based on the joint use of spatial and temporal features. Psychophysiology 48 (2), 229–240. doi:10.1111/j.1469-8986.2010.01061.x.

Oleszkiewicz, A., Schriever, V.A., Croy, I., Hähner, A., Hummel, T., 2019. Updated Sniffin' Sticks normative data based on an extended sample of 9139 subjects. Eur. Arch. Oto-Rhino-Laryngol. 276 (3), 719–728. doi:10.1007/s00405-018-5248-1.

Olofsson, J.K., Broman, D.A., Gilbert, P.E., Dean, P., Nordin, S., Murphy, C., 2006. Laterality of the olfactory event-related potential response. Chem. Sens. 31 (7), 699–704. doi:10.1093/chemse/bjl011.

Oostenveld, R., Delorme, A., & Makeig, S. (2003). *DIPFIT: equivalent dipole source localization of independent components.* http://sccn.ucsd.edu/wiki/A08:_DIPFIT

Oostenveld, R., Praamstra, P., 2001. The five percent electrode system for high-

resolution EEG and ERP measurements. Clin.Neurophysiol. 112, 713–719. doi:10.1016/S1388-2457(00)00527-7.
Peirce, J.W., 2007. PsychoPy — psychophysics software in python. J. Neurosci. Methods 162 (1), 8–13. doi:10.1016/j.jneumeth.2006.11.017.
Peirce, J.W., 2009. Generating stimuli for neuroscience using PsychoPy. Front. Neuroinform. 2, 10. doi:10.3389/neuro.11.010.2008.
Pion-Tonachini, L., Kreutz-Delgado, K., Makeig, S., 2019. ICLabel: an automated electroencephalographic independent component classifier, dataset, and website. NeuroImage 198, 181–197. doi:10.1016/j.neuroimage.2019.05.026.
Porter, J., Craven, B., Khan, R.M., Chang, S.J., Kang, I., Judkewitz, B., Volpe, J., Settles, G., Sobel, N., 2007. Mechanisms of scent-tracking in humans. Nat. Neurosci. 10 (1), 27–29. doi:10.1038/nn1819.
Rajan, R., Clement, J.P., Bhalla, U.S., 2006. Rats smell in stereo. Science 311 (5761), 666–670. doi:10.1126/science.1122096.
Rombaux, P., Guérit, J.M., Mouraux, A., 2008. Lateralisation of intranasal trigeminal chemosensory event-related potentials. Neurophysiol. Clin. 38 (1), 23–30. doi:10.1016/j.neucli.2007.12.002.
Schifferstein, H.N.J., Smeets, M.A.M., Postma, A., 2009. Comparing location memory for 4 sensory modalities. Chem. Sens. 35 (2), 135–145. doi:10.1093/chemse/bjp090.
Schriever, V.A., Han, P., Weise, S., Ho, F., Pellegrino, R., Hummel, T., 2017. Time frequency analysis of olfactory induced EEG-power change. PLoS ONE 1–11.
Shusterman, D., 2009. Qualitative effects in nasal trigeminal chemoreception. Ann. N.Y. Acad. Sci. 1170 (1), 196–201. doi:10.1111/j.1749-6632.2009.03928.x.
Smeets, M.A.M., Kroeze, J.H.A., Dalton, P.H., 2006. Setting occupational exposure limits in humans: contributions from the field of experimental psychology. Int. Arch. Occup. Environ. Health 79 (4), 299–307. doi:10.1007/s00420-005-0053-8.
Sorokowski, P., Karwowski, M., Misiak, M., Marczak, M.K., Dziekan, M., Hummel, T., Sorokowska, A., 2019. Sex differences in human olfaction: a meta-analysis. Front. Psychol. 10 (FEB), 1–9. doi:10.3389/fpsyg.2019.00242.
Stuck, B.A., Frey, S., Freiburg, C., Hörmann, K., Zahnert, T., Hummel, T., 2006. Chemosensory event-related potentials in relation to side of stimulation, age, sex, and stimulus concentration. Clin. Neurophysiol. 117 (6), 1367–1375. doi:10.1016/j.clinph.2006.03.004.
Tzourio-Mazoyer, N., Landeau, B., Papathanassiou, D., Crivello, F., Etard, O., Delcroix, N., Mazoyer, B., Joliot, M., 2002. Automated anatomical labeling of activations in SPM using a macroscopic anatomical parcellation of the MNI MRI single-subject brain. NeuroImage 15 (1), 273–289. doi:10.1006/nimg.2001.0978.
van Thriel, C., Schäper, M., Kiesswetter, E., Kleinbeck, S., Juran, S., Blaszkewicz, M., Fricke, H.H., Altmann, L., Berresheim, H., Brüning, T., 2006. From chemosensory thresholds to whole body exposures - experimental approaches evaluating chemosensory effects of chemicals. Int. Arch. Occup. Environ. Health 79 (4), 308–321. doi:10.1007/s00420-005-0057-4.
van Vliet, M., Liljeström, M., Aro, S., Salmelin, R., Kujala, J., 2018. Analysis of functional connectivity and oscillatory power using DICS: from raw MEG data to group-level statistics in python. Front. Neurosci. 12. https://www.frontiersin.org/articles/10.3389/fnins.2018.00586.
Welge-Lüssen, A., Looser, G.L., Westermann, B., Hummel, T., 2014. Olfactory source localization in the open field using one or both nostrils. Rhinology 52 (1), 41–47. doi:10.4193/Rhino13.108.
Yang, A.I., Dikecligil, G.N., Jiang, H., Das, S.R., Stein, J.M., Schuele, S.U., Rosenow, J.M., Davis, K.A., Lucas, T.H., Gottfried, J.A., 2021. The what and when of olfactory working memory in humans. Curr. Biol. 31 (20), 4499–4511. doi:10.1016/j.cub.2021.08.004, e8.
Yücel, M.A., Selb, J., Aasted, C.M., Petkov, M.P., Becerra, L., Borsook, D., Boas, D.A., 2015. Short separation regression improves statistical significance and better localizes the hemodynamic response obtained by near-infrared spectroscopy for tasks with differing autonomic responses. Neurophotonics 2 (3), 035005. doi:10.1117/1.NPh.2.3.035005.
Zeileis, A., Hornik, K., Wiel, M.A., Hothorn, T., 2008. Implementing a class of permutation tests: the coin package. J. Stat. Softw. 28 (8), 1–23.